RSC Advances

This is an *Accepted Manuscript*, which has been through the Royal Society of Chemistry peer review process and has been accepted for publication.

Accepted Manuscripts are published online shortly after acceptance, before technical editing, formatting and proof reading. Using this free service, authors can make their results available to the community, in citable form, before we publish the edited article. This *Accepted Manuscript* will be replaced by the edited, formatted and paginated article as soon as this is available.

You can find more information about *Accepted Manuscripts* in the Information for Authors.

Please note that technical editing may introduce minor changes to the text and/or graphics, which may alter content. The journal's standard Terms & Conditions and the Ethical guidelines still apply. In no event shall the Royal Society of Chemistry be held responsible for any errors or omissions in this *Accepted Manuscript* or any consequences arising from the use of any information it contains.

ROYAL SOCIETY OF CHEMISTRY

www.rsc.org/advances

Journal Name

RSCPublishing

ARTICLE

Amplified Electrochemical Genotyping of Single-Nucleotide Polymorphisms using Graphene-Gold Nanoparticles Modified Glassy Carbon Platform

Cite this: DOI: 10.1039/xoxxoooooox

Received ooth January 2012,
Accepted ooth January 2012

DOI: 10.1039/xoxxoooooox

www.rsc.org/

Seyyed Mehdi Khoshfetrat and Masoud A. Mehrgardi*[a]

The main challenges in the construction of DNA biosensors for genotyping of all possible Single-Nucleotide Polymorphisms (SNPs) are their sensitivity, speed and expenses. The application of nanoparticle-modified monobases for electrochemical genotyping of SNPs has been investigated in our previous study. In the present manuscript, that strategy was modified by applying graphene-gold nanoparticle (GR-AuNPs) nanocomposite to achieve further amplification and higher sensitivity of SNPs genotyping. The present strategy shows good potential to sensitive discriminate, quantify and genotyping different SNPs. Taking the advantages of triple-amplification effects of the AuNPs, GR and Modified Metal (Au and Ag) Nanoparticles, this DNA biosensor exhibits a highly sensitive responses for the genotyping of different SNPs and detection of thermodynamically stable SNP (G-T) and A-C mismatch targets in the range of 10-1700 pM and 20-1200 pM with the detection limits of 2 and 10 pM (3σ) for G-T and A-C mismatch targets, respectively. The results demonstrate while the surface coverage of DNA per unit area just slightly increases, but with dramatic increase in the active surface area, the absolute loading amount of DNA on the surface would also be increased.

1. Introduction

There is an urgent need to develop sensitive, selective, and rapid strategies for SNP detection in mammalian genetics as well as in clinical practices. SNPs are single-base mutations that can occur in coding regions and may lead to major health problems, genetic diseases and altered response to drug treatments [1]. Applications of different SNP genotyping technologies, in biomedical areas and clinical diagnostics, have been thoroughly discussed in a number of excellent reviews [2-4]. Moreover, High-throughput genotyping is traditionally done using next-generation sequencing[5-7] as a sensitive diagnostic method. However, this technique is relatively costly, time consuming and labor intensive. Among these technologies, electrochemical genosensors offer a promising alternative to carry out applications of SNPs analysis due to their low cost, miniaturization, high sensitivity, and compatibility with micro-fabrication technology [8-10]. Development of methods, that require more sensitive, inexpensive and simpler protocols, is very important in genotyping of different SNPs and while electrochemical genosensore for the coding of SNPs possess the mentioned characteristics, up to now, they have been reported just only in few manuscripts. Also, in order to meet the increasing demand for ultrasensitive biosensing for detection of low-abundance SNPs, various signal amplification strategies including application of enzymes [11], apoferritin [12, 13], liposomes [14], nanoparticles [15, 16], quantum dots [17, 18], have been employed. Willner's group have used monobase-modified alkaline phosphatase enzyme and also liposome for the detection of single base mutations [11, 14]. Liu and Lin [12] have described the novel quantitation of SNPs using monobase-modified cadmium phosphate loaded apoferritin. However, the enzyme or protein-based detections are limited due to the denaturation, the leakage of nanoparticles, high cost and time-consuming purification process. Monobase-modified gold nanoparticle, as a redox probe, has been used by the Kerman's group for SNPs genotyping [15]. However, the electrochemical oxidation of AuNPs occurs at a high positive potential, close to guanine and adenine oxidation, that can limit the precision and selectivity of the assay [19]. In another reported strategy for the coding of SNPs, Zhang and his co-workers [17] have proposed a method for the detection of point mutation using different single-base-

RSC Advances Accepted Manuscript

coded quantum dot (QD) nanoparticle. In these methods, despite the advanced detection strategies, relatively little progresses in electrochemical simultaneous genotyping of multiple significant genetic variations have been carried out. Subsequently, different nanocrystals quantum dots [18], apoferritin-different metal nanoparticles [13], monobase-modified silver and gold nanoparticles [16] have been investigated. However, the QD-based detections need complicated syntheses and necessitated severe detection conditions such as nanocrystals dissolution and high potential accumulations which are not suitable for the routine analyses. Other critical points to achieve further sensitivity of the biosensors are the reduction of background current to improve signal-to-background ratio in one side and also increase of the loading amount of self-assembled sensing monolayer on the other side. The Graphene oxide (GO) and GR along with silver and gold nanoparticles (Ag/AuNPs) have received tremendous attention owing to the unique properties of such as excellent conductivity, high surface area, catalytic properties, electron transfer enhancement, their non-toxic nature and good biocompatibility. Therefore, they have been applied in the designing and fabrication of different electrochemical immunosensors and DNA sensors to amplify the analytical signals [20-26]. For example, Zhang's group reported an electrochemical DNA hybridization biosensor using gold nanorods (Au NRs) and graphene [27, 28]. GR−AuNPs have been also used for the detection of oxygen reduction and glucose [29, 30], dopamine [31], Phoxim [32], Carbamazepine [33], sumatriptan [34], thrombin[35], bisphenol A [36], ractopamine [37] and nitrite [38].
Electrodeposition technique is an effective and simple method for synthesizing of metal or alloy NPs [39]. On the other side, recently, the electrochemical reduction of GO to GR as an effective tool, because of its fast, green and non-toxic solvents, has also drawn great attention [40]. Therefore, electrodeposition of metal NPs has been used for higher loading of different NPs on the GR-modified electrode [41, 42]. Our group recently reported electrochemical simultaneous SNPs genotyping using monobase-conjugated modified nanoparticles on a single platform [16]. Also, in another study, dual amplification SNPs using nanoporous gold electrode and GO was recently reported by our group [43]. In continuation of our previous study, to amplify the signal, a sensing platform for ultrasensitive, selective, and efficient detection of SNPs based on graphene-AuNPs modified glassy carbon electrode (GR-AuNPs/GCE) has been developed. Herein, for genotyping of individual SNPs, the same strategy that has been developed in our research group [16]. Briefly, The GR was immobilized on a pretreated GCE, firstly. Then AuNPs electrochemically deposited on the GR modified GCE (GR/GCE) for the effective and directional immobilization of sensing interface (probe oligunocleotide) via gold-sulfur chemistry. SNPs are detected by electrooxidation of AgNPs and DABA as a signal tracer in the presence of DNA polymerase I (Klenow fragment), as an induced coupling of monobases to mismatches. Triple signal amplification for electrochemical SNPs genotyping was developed by the following processes: 1) the GR accelerate the electron transfer rate [19, 44] 2) the AuNPs increasing the surface area to loading high-content of sensing interface because of the intrinsic property of high surface-to-volume ratio of AuNPs and the GR-AuNPs hybrid as a sensing platform has a synergetic effect to improve the performance and 3) large amount of AgNPs and DABA as signal tracers prompt the sensitivity. To demonstrate the substantial role of GR in signal amplification, the signals of the business based on amps/GCE and GR-AuNPs/GCE platforms have been compared and exhibited much higher electrochemical performance that can be attributed to the high surface area and the excellent electrical properties of GR.

2. Experimental

2.1. Materials and apparatus

The synthetic oligonucleotides were purchased from Eurofins MWG/Oberon Co. with the following sequences (5′ to 3′):

Probe	SH-$(CH_2)_6$- CTG CGT TTT
Complementary	TGC CGA AAA AAA ACG CAG
A-C mismatch	T**A**C CGA AAA AAA ACG CAG
G-T Mismatch	TGC **T**GA AAA AAA ACG CAG
Capture	TTT TCG GCA

Tris(2-carboxyethyl)phosphine (TCEP), Tris–HCl, Sodium hydroxide (NaOH), sodium chloride (NaCl), potassium chloride (KCl), potassium nitrate (KNO_3), magnesium chloride ($MgCl_2$), potassium dihydrogen phosphate (KH_2PO_4), disodium hydrogen phosphate (Na_2HPO_4), hydrochloric acid (HCl), sulfuric acid (H_2SO_4), N-Hydroxysuccinimide (NHS), N-(3-Dimethylaminopropyl)-N′ ethylcarbodiimide hydrochloride (EDC), potassium ferrocyanide ($K_4[Fe(CN)_6]$), potassium ferricyanide ($K_3[Fe(CN)_6]$), sodium borohydride ($NaBH_4$), 3,4-diaminobenzoic acid (DABA), ruthenium hexamine trichloride (RuHex), cysteine (Cys.), Cysteamin hydrochloride (Cyt-HCl), potassium permanganate ($KMnO_4$), hydrogen peroxide (H_2O_2) and silver nitrate ($AgNO_3$) were purchased from commercial companies (Sigma Aldrich or Merck). The stock solutions of the oligonucleotides were prepared with 1X phosphate buffer solution (PBS 1X) pH 7.4 (0.01 M Na_2HPO_4, 2 mM KH_2PO_4, 0.15 M NaCl and 0.15 M KCl,). Adenosine 5′-triphosphate (ATP), cytidine 5′-triphosphate (CTP), guanosine 5′-triphosphate (GTP), thymidine 5′-triphosphate (TTP) and DNA polymerase I (Klenowfragment), were purchased Vivantis Co. (Malaysia). Monobase solutions were prepared using a 20 mM Tris–HCl buffer solution containing (TBS) 20 mM NaCl (pH 7). A conventional electrochemical cell consists of the modified glassy carbon electrode (GCE) in connection to Ag/AgCl (3 M KCl) and Pt wire, as the working electrode, reference and the counter electrode were used, respectively. The electrochemical impedance spectroscopy (EIS) and cyclic voltammetry (CV) were carried out using an Autolab PGSTAT30 in the solution containing of $K_3[Fe(CN)_6]/K_4[Fe(CN)_6]$ (1:1, 0.5 mM), as the redox couple. The EIS measurements were performed by applying an AC

RSC Advances Accepted Manuscript

 This journal is © The Royal Society of Chemistry 2012

potential with signal amplitude of 5 mV and frequency range over 10 kHz to 0.1 Hz, at the open circuit potential (OCP). Differential pulse voltammetry (DPV) was used to electrochemical genotyping SNPs and quantification of thermodynamically G-T and A-C mismatches over a range of -0.2 to 0.6 V at the scan rate of 20 $mV.s^{-1}$ and the pulse amplitude of 25 mV. Field emission scanning electron microscopy (FE-SEM) was accomplished on a Mira 3-XMU at an accelerating voltage of 20 kV. X-ray diffraction (XRD) patterns of the samples were recorded on a Bruker D8/Advance X-ray diffractometer with Cu-K_α radiation at 40 kV and 40 mA. Raman spectra were collected on a SENTERRA Raman spectrometer using 745 nm laser excitation. X-ray photoelectron spectroscopy (XPS) analysis was carried out using a VG Microtech Twin anode XR3E2 X-ray source and a concentric hemispherical analyzer operated at a base pressure of 5×10^{-10} mbar using Al K_α ($h\upsilon$=1486.6 eV).

2.2. Procedure of Electrochemical genotyping of SNP

2.2.1. Preparation of the GR-AuNPs/GCE or AuNPs/GCE:

Prior the preparation of modified electrode, GCE was mechanically polished with 1, 0.3, and 0.05 µm alumina powder sequentially to a mirror finish. For the preparation of GR-AuNPs/GCE, primarily 10 µl of 0.5 $mg.mL^{-1}$ exfoliated GO was casted on the GCE surface, and electrochemical reduction of GO was performed to prepare GR/GCE by potential scanning between 0 and −1.5 V for 25 cycles in pH 4.0 PBS [40]. Then, the GR/GCE was immersed in the solution containing 0.01 $g{\cdot}L^{-1}$ $HAuCl_4$ and 0.1 M KNO_3 as a supporting electrolyte for electrodeposition of AuNPs at the constant potential -0.2 V for 90 s under magnetic stirring. For comparison AuNPs/GCE, GCE surface was similarly treated in the absence of GR.

2.2.2. Electrochemical genotyping:

After providing of the platforms, the biorecognition layers have been prepared using the same strategy that have been previously developed by our group [16, 43]. The surface coverage of DNA on the surface has been obtained using chronoculometry. Characterization of surface platform for immobilization of different DNA was performed by EIS and voltammetric techniques.

3. Results and discussion

Graphene oxide (GO) was synthesized from graphite powder by a modified Hummer's method [45] as we reported in our previous manuscript [43]. Cysteine and Cysteamine-modified silver and gold nanoparticles, respectively, were also prepared using our previous study [16]. Monobase-coded Nanoparticles (M-NPs) probes, including thymidine-coded AgNPs (T-AgNPs), guanosine-coded AgNPs (G-AgNPs), cytidine-coded DABA-modified AuNP (C-Au-DABA), Adenosine-coded DABA-modified AuNP (A-Au-DABA) and guanosine-coded DABA-modified AuNP (G-Au-DABA) were prepared via phosphoramidate bond of 5′-phosphate group of monobases with the free amino groups of the immobilized Cysteine and Cysteamine on the surface of AgNPs and AuNPs, respectively [16].

3.1. Characterization of modified GCE

Fig. 1A shows XRD patterns of the pristine graphite, GO, GR and GR-AuNPs. The diffraction peak of exfoliated GO with inter-distance (d-spacing) of 7.75 A° appears at 11.4° (002). In Comparison to the pristine graphite, this value is larger than the d-spacing (3.35 A°) of pristine graphite (2θ=26.6°) due to the presence of oxygen containing functional groups [40]. After electrochemical reduction of GO, the diffraction peak of GR is at 26.6°, similar to the previously reported results [40]. The XRD pattern shows obvious peaks located at 2θ values of 39.6, 46.3, 67.4 and 81.4° corresponding to the (111), (200), (220), and (311), respectively confirming the presence of AuNPs on the GR/GCE, and thus, formation of GR-AuNPs hybrid with the extensive conjugated sp^2 carbon networks, represented by peak located at 26.2°, which is corresponded to the interlayer spacing of 3.4 A° [46]. As shown in Fig. 1B, the Raman spectrum of GO contained both D and G bands at 1360 and 1585 cm^{-1} which are representatives of sp^3 and sp^2 carbon hybridization, respectively. After electrochemically reduction of the exfoliated GO, the intensity of D band and ratio of D/G as well are increased, due to a decrease in the average size of sp^2 carbon domains of GO [40]. Fig. 1C and show the SEM image of GR-AuNPs, which shows AuNPs are uniformly covered on the GR with average size of 20 nm.

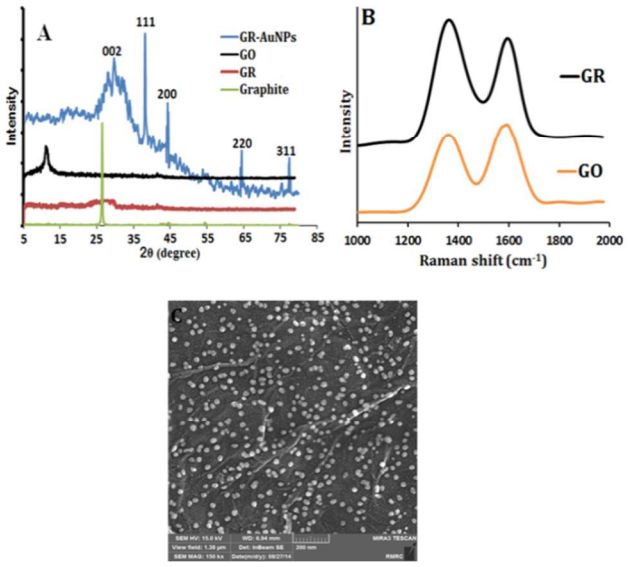

Fig. 1. XRD pattern of graphite, GO, GR and GR-AuNPs (A), Raman spectra GO and GR (B), SEM image of GR-AuNPs (C).

RSC Advances Accepted Manuscript

The chemical and the content elemental composition were characterized using XPS [47]. The XPS survey spectrum of GR-AuNPs nanocomposite shows the distinct Au 4f, C 1s and O 1s peaks (Fig. 2A), without any other impurities [48, 49]. The high-resolution deconvoluted C1s spectrum of GO (Fig. 2B) and GR (Fig. 2C) samples, respectively, reveals the presence of C-C (284.3 eV), C-O (286.3 eV), C=O (287.7 eV), and O-C=O (289.0 eV) [45, 50]. Although, the C 1s XPS spectra of GR and GO also exhibit the same species, the peak intensities of oxide species in the GR are much weaker than those in the spectrum of GO. These results confirm that the O/C ratio in the exfoliated GO (32.5%) compared to GR (7.8%), remarkably decreases after the electrochemical reduction, i.e., ~76% of the most of epoxide and hydroxyl functional groups has been removed successfully during the electrochemical reduction. The XPS analysis has been performed on GR-AuNPs nanocomposite platform to obtain the content and information about the oxidation state of AuNPs [51, 52]. Fig. 2D shows a pair of doublet peaks at 85.3 and 89.1 eV , which are corresponded to metallic Au atoms (Au^0). Furthermore, the absence Au^+ species peaks at 86.2 and 89.9 eV demonstrates that AuNPs is in metallic form on the GCE surface. The AuNPs content in the GR-AuNPs nanocomposite platform is ~16.3%, as estimated from the XPS data.

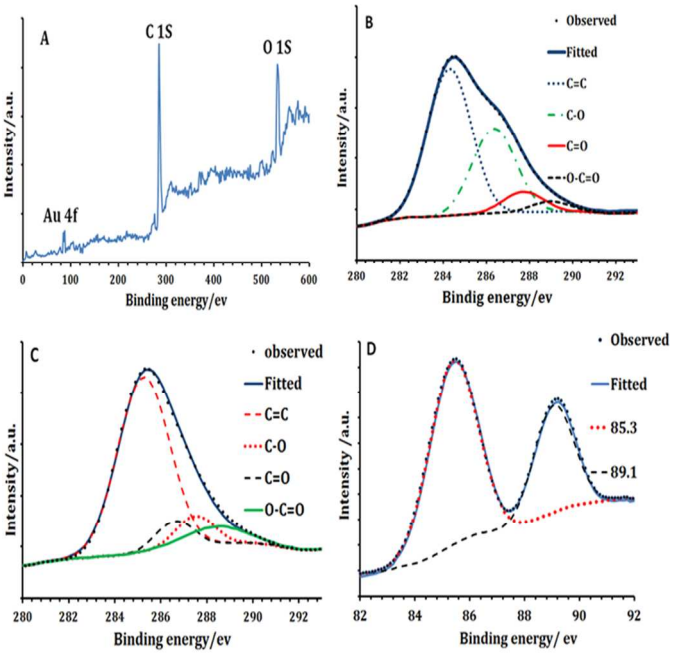

Fig. 2. XPS spectra of GR-AuNPs nanocomposite (A), High-resolution of C 1s XPS spectra of GO (B) and GR (C) and Au 4f region (D).

3.2. Electrochemical performance of different modified electrodes

In order to confirm the modified GCE has been constructed successfully, each modification step was investigated using CV and EIS experiments. The CVs were recorded over range of

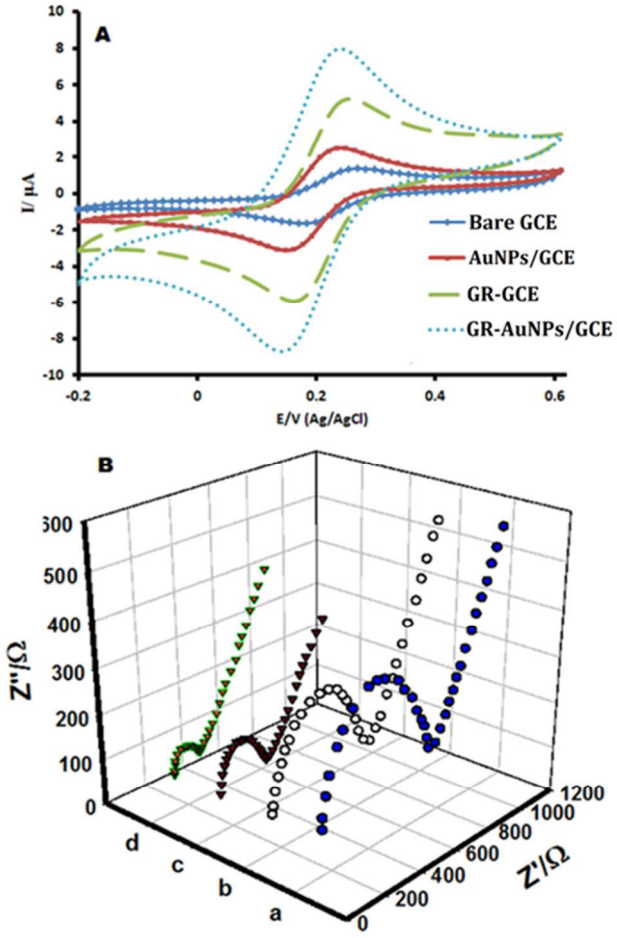

Fig. 3. (A) CVs of different GCE modification steps in the presence of 0.5mM $[Fe(CN)_6]^{3-}/[Fe(CN)_6]^{4-}$ (equimolar) at a scan rate of 100 $mV.s^{-1}$. (B) EIS of 0.5mM $[Fe(CN)_6]^{3-}/[Fe(CN)_6]^{4-}$ (equimolar) for different modified electrodes (a) bare GCE, (b) AuNPs/GCE, (c) GR/GCE and (d) GR-AuNPs/GCE.

−0.2 V to +0.6 V in a solution containing of $[Fe(CN)_6]^{3-/4-}$on the bare GCE, GR/GCE, AuNPs/GCE and GR-AuNPs/GCE, respectively, as shown in Fig. 3A. For bare GCE, a pair of well-defined peak with ΔE_p=79 mV is observed. However, the peak currents of redox probe are increased in each modification step of GCE with GR, AuNPs and GR-AuNPs, respectively. Also, the largest peak currents and reversible behavior (ΔE_p <65 mV) are related to the GR-AuNPs/GCE, indicating the electron transfer rate is increased on GR-AuNPs/GCE. Moreover, the corresponding electrochemical impedance spectra of different modified electrodes were studied. Fig. 3B shows the impedance spectra after each GCE modification step. The R_{ct} of the redox probe on the bare GCE (spectrum a) is 720 Ω. After modification of GCE with AuNPs, GR and GR-AuNPs composite (spectra b, c and d, respectively) the R_{ct} decrease to 630, 360 and 250 Ω and therefore, faster electron transfer rates in compared to bare GCE are observed, which are in

RSC Advances Accepted Manuscript

This journal is © The Royal Society of Chemistry 2012

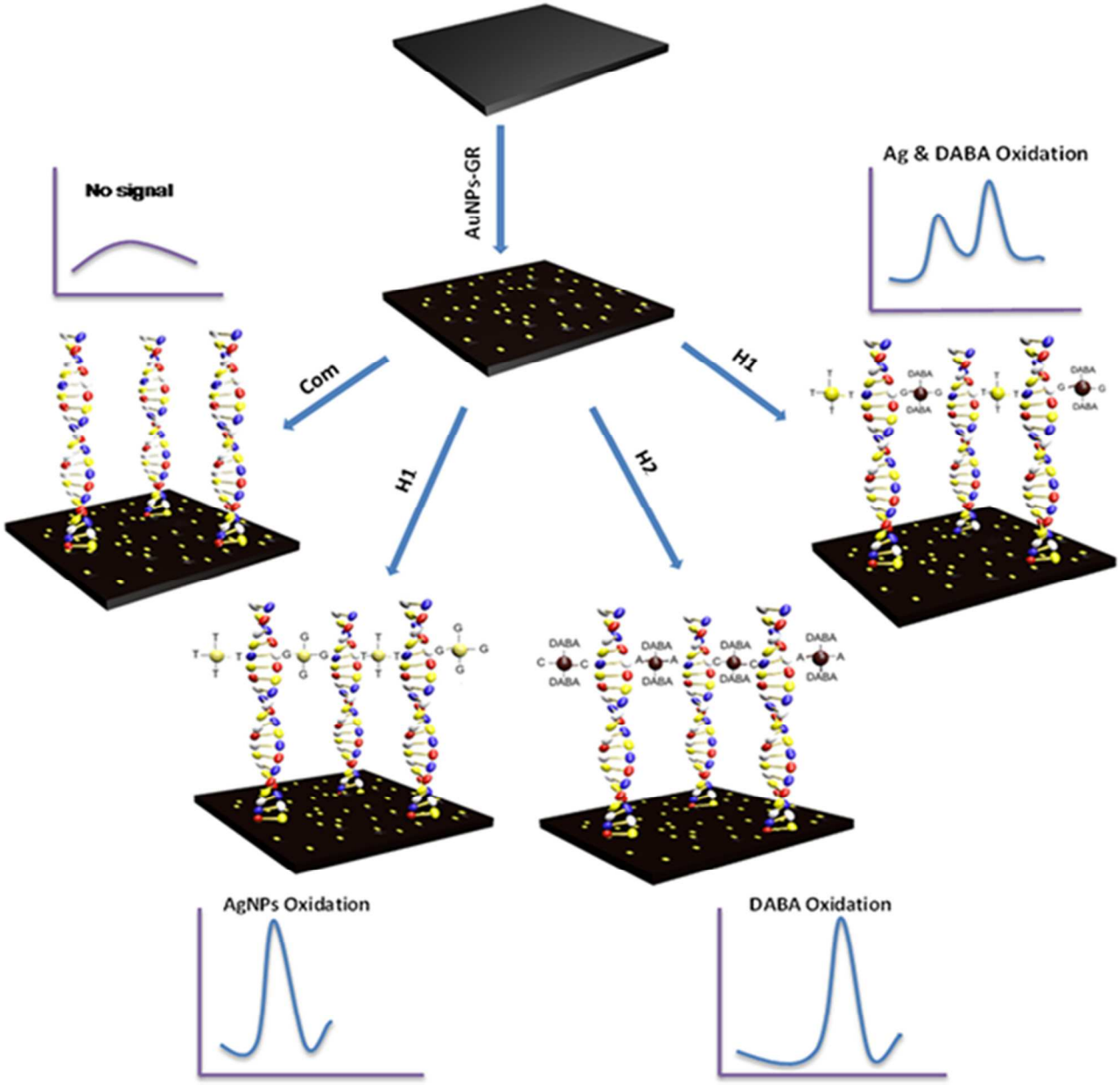

Scheme 1. Schematic illustration of amplified electrochemical genotyping of different SNPs.

accordance with the result of CVs. Especially, when AuNPs are electrochemically deposited on the surface of the GR/GCE, the R_{ct} of GR-AuNPs/GCE are decreased even more than GR/GCE and AuNPs/GCE, which suggesting the synergistic effect of AuNPs and GR. These results suggest that GR-AuNPs/GCE can provide a unique platform for genotyping of mismatches.

3.3. Electrochemical genotyping of different mismatches

The general concept for the amplified detection of a single-base mismatch in the DNA is illustrated in Scheme 1. After electrodeposition of GR and AuNPs on the GCE, the hybridization of the immobilized probe on the GR-AuNPs/GCE with the different concentration of mutant (A-C and G-T) or complementary targets generate the respective double-stranded form on the electrode surface. Finally, non-hybridized section of the target is hybridized with the capture strand. Now, the resulted structure is treated by M-NPs, leading to the hybridization of M-NPs with the mutant sites and no interaction in the presence of complementary target. The assembled probe on the modified electrode surface was examined by chronocoulometric method [53], showing the surface coverage of 4 (±0.5) × 10^{12} molecules/cm^2. While the surface coverage of

RSC Advances Accepted Manuscript

the electrode by DNA probe per unit area does not change significantly, by increasing the surface area by applying GR-AuNPs, the loading amount of the probe on the surface is increased.

Since density of AuNPs onto GCE strongly influences on the detection sensitivity of the genosensor, it is of key importance. In order to investigate the density of the AuNPs on the electrode responses, electrodeposition of AuNPs on the GR/GCE was carried out at different deposition times. By increasing the density of AuNPs, the analytical signals of the genosensor in the presence of mismatched targets increase and reach to the maximum amount at the deposition time of 90 s (Fig. S1, curve c, supplementary information). However, further increasing of the deposition times not only do not increase the analytical signals, but also lead to the decreases in the electrooxidation currents of AgNPs and DABA (Fig. S1, curve d, supplementary information). It can be attributed to the increases of the nanoparticle sizes and their aggregations together and therefore it leads to decrease in the loading amount of DNA and subsequently lower loading amounts of molecular reporters, i.e. AgNPs and DABA molecules on the surface.

Fig. 4 shows a set of DP voltammograms for the detection of A-C and G-T mismatches. As expected by the binding events in Scheme 1, A-C and G-T mismatches are hybridized with their complementary bases in modified M-NPs, i.e., with T-AgNPs/G-AgNPs and C-Au-DABA/A-Au-DABA, respectively. After the A-C modified electrode was subjected to T-AgNPs/G-AgNPs, a well-defined oxidation peak of AgNPs is observed, because of the hybridization of Adenosine and Cytosine bases of A-C mismatch with complementary bases of T and G and accumulation of AgNPs on the electrode surface. Also, the electrooxidation of DABA was followed for genotyping of G-T mismatches after coding by C-Au-DABA/A-Au-DABA. Fig. 4 compares the DPV responses of electrooxidation of signal tracers on the bulk gold electrode [16], AuNPs/GCE and GR-AuNPs/GCE for genotyping of A-C and G-T mismatches. As shown in Fig. 4A, genotyping of A-C mismatches on the AuNPs/GCE , the anodic peak current (Ip_a) of AgNPs is found to be 1.6 μA, while, the GR-AuNPs/GCE gives Ip_a 3.4, around 2 higher than that of the AuNPs/GCE. Also, the comparison between the anodic peak currents of this protocol and our previously reported on the bulk gold electrode [16] demonstrates the signal has been amplified 3.2 times at the same concentration (800 pM).

Also, the electrooxidation of DABA was monitored after treatment of G-T mismatch-modified electrode with C-Au-DABA/A-Au-DABA (Fig. 4B). The differential voltammogram of DABA accumulated on the bulk gold electrode after modification with 800 pM G-T mismatches shows a small response, whereas hybridization of AuNPs/GCE modified electrode with the same concentration of G-T mismatch targets shows a relatively higher peak current. To demonstrate the efficiency of genotyping to improve the detection sensitivity, the GR-AuNPs/GCE was also used as modified the platform and displayed much higher peak current. The high performance response of GR-AuNPs nanocomposite platform can be attributed the combination of the following factors: 1) Higher loading amount of DNA probe using AuNPs. 2) The electrical network of AuNPs through their direct incorporating with the GR [29]. 3) Much easier accessibility of M-NPs to mutant sites

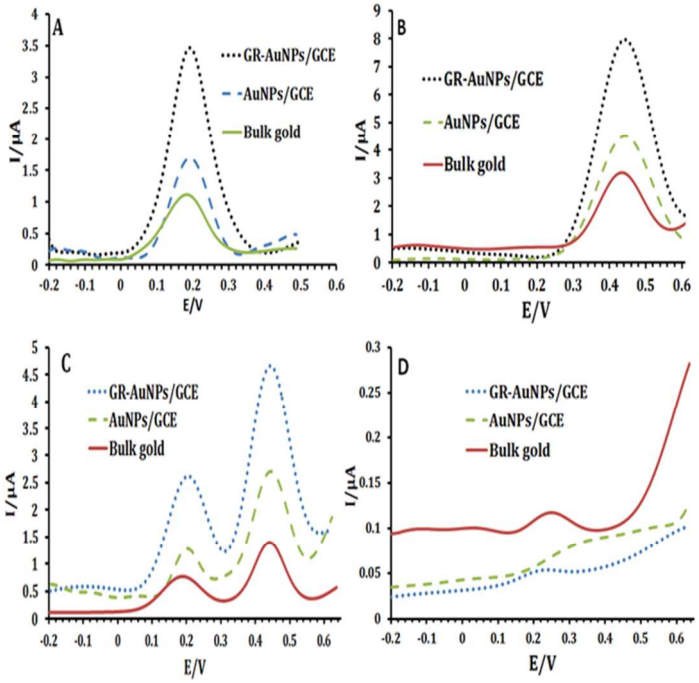

Fig. 4. (A) Electrooxidation of AgNPs for genotyping of A-C mismatch target; (B) Electrooxidation of DABA for genotyping of G-T mismatch target (C) Simultaneous genotyping of A-C mismatches after interaction with T-AgNPs/G-Au-DABA. (D) Complementary target in the presence of T-AgNPs/G-Au-DABA (on bulk gold, AuNPs/GCE and GR-AuNPs/GCE surfaces).

and 4) High-efficient electron acceleration of the GR [54]. GR sheets serve as the electron acceptor and transporter [55, 56]. Therefore, the well-distributed AuNPs on the surface of graphene would induce more active sites for the immobilization of molecular reporters. Moreover, this leads to an efficient electrical network through their direct incorporating with GR. On the other hand, by electrodeposition of GR on the GCE, the electrode surface reveals a thin layer with typical crumpled and wrinkled structure [57]. Therefore AuNPs are electrochemically deposited on uneven surface in compared to smooth bare of GCE. It causes that the DNA probe and subsequently, the hybridization of targets and capture are performed in different layers and the accessibility of M-NPs to mutant sites on the mismatch targets would be much easier. Consequently, the larger amounts of M-NPs are accumulated on the mismatch-modified electrode and leads to higher response currents. Moreover Xu et al. [54] recently approved, when the GO the electrochemically reduction to GR has much higher electron transfer rate in comparison with chemically reduction of GO. The fast electron transfer should be attributed to edge effect of GR due to crumpled and wrinkled structure.

The oxidation potential of AgNPs and DABA are completely separated (0.2 and 0.44 V respectively) and it would be expected the biosensor can be used for simultaneous different SNPs genotyping by AgNPs and DABA. For this purpose, e.g. A-C mismatches, the modified electrode treated with T-AgNPs/G-Au-DABA (Fig. 4C). The treatment of the electrode to the T-AgNPs and G-Au-DABA simultaneously, shows well-resolved oxidation signals of AgNPs and DABA. Fig. 4D

RSC Advances Accepted Manuscript

This journal is © The Royal Society of Chemistry 2012

Journal Name

RSCPublishing

ARTICLE

Table 1. Comparison between the present study and other previously reported biosensors for genotyping of SNPs.

Method[a]	Technique/Type of mismatch[b]	Detection limit	Ref.
Monobase-modified AuNPs	SWV/ All of the SNPs	29.75 pmol	[15]
G-modified Cd-ApoNPs	SWV/ CC mismatches	0.3 pM	[12]
Monobase-coded CdS	QCM/ All of the SNPs	-	[17]
Monobase-modified QDs	SWV/ All of the SNPs	-	[18]
Monobase-modified Metal-ApoNPs	SWV/ All of the SNPs	5 pM (in case of A-G mismatch)	[13]
Single base extension	SPR/ A-C mismatches	100 pM	[58]
Surface ligation reaction	LSAV/ A-G mismatches	2 pM	[59]
Peptide nucleic acid-based methods	SERS/ A-G mismatches	3.4 pM	[60]
Mismatch binding protein-based	QCM / T-G mismatches	1 nM	[61]
Mismatch binding protein-based	Fluorescence/ All of the SNPs	5 nM (in the case of G-T mismatches)	[62]
Molecular beacon-based	Amperometry/ G-G mismatches	0.1 nM	[63]
Molecular beacon-based	Fluorescence	40 pM	[64]
Exonuclease based	Impedance/ C-C	42 pM	[65]
Monobase-Conjugate Nanparticles on gold electrode	DPV/ All of the SNPs	5 pM (in case of G-T mismatch)	[16]
Modified Nanoparticles on Gold Nanoparticles-Graphene	DPV/ All of the SNPs	2 and 10 pM (for G-T and A-C mismatch targets)	**Present study**

[a] ApoNPs, Apoferritin nanoparticles; QC, Quantum dot.

[b] SWV, Square wave voltammetry; QCM, Quartz crystal microbalance; SPR, Surface Plasmon resonance; LSAV, Leaky surface acoustic wave; SERS, Surface-enhanced Raman spectroscopy; DPV, Differential pulse voltammetry.

shows the modified platforms in the presence of completely complementary DNA when the exposure with T-AgNPs/G-Au-DABA. No obvious signals can be observed on the different modified electrodes, especially on the GR-AuNPs/GCE platform, that demonstrates the effect of non-specific adsorption of M-NPs could be ignored. The distinct differences are observed in DPV responses between the complementary DNA and the A-C point mutation after adding T-AgNPs/G-Au-DABA to DNA duplex. These results imply that the hybridization has taken place through the specific base-pairing. Moreover, the intensity of currents in A-C and G-T mismatch targets when treated with T-AgNPs/G-AgNPs (Fig. 4A) and C-Au- DABA/A-Au-DABA (Fig. 4B) respectively, is almost twice the signal of A-C mismatches when the simultaneous detection is carried out (Fig. 4C) (treated with T-AgNPs/G-Au-DABA). It is worthy to note that the background signals of the biosensor are not increased significantly by applying GR-AuNPs/GCE as the biosensor platform resulting improvement of signal-to-noise in compare to bulk gold electrode.

Fig. 5 illustrates the comparison between electroxidation of AgNPs and DABA at the same concentration of A-C and G-T mismatches (800 PM), respectively on the GR-AuNPs/GCE platform. As shown in Fig. 5, the proposed electrochemical biosensor using DABA as a signal tracer exhibited a larger current shift ($\sim\Delta I$=3 μA) in comparison to AgNPs. Cysteamin-modified AuNPs was used as a carrier for DABA tracers. While G-T mismatch targets form more thermodynamically stable double [66, 67] strand form and the hybridization efficiency are much higher than A-C mismatch targets, since numerous DABA could be loaded on the surface of AuNPs, it leads to better analytical signal performance. Although oxidation signal of AuNPs can be directly used as an analytical signal, their electrochemical oxidation occurs at relatively high potential. In contrast, AgNPs oxidized at more moderate potential which resulted to obviate of interferences species and owing to

RSC Advances Accepted Manuscript

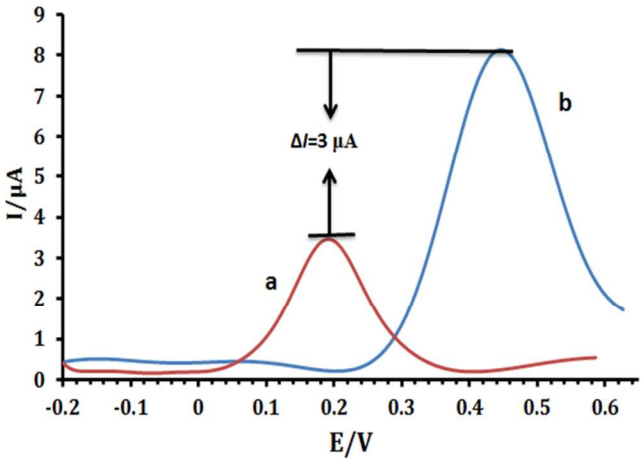

Fig. 5. Comparison between electrooxidation of AgNPs (a) and DABA (b) on the GR-AuNPs/GCE surface.

relatively sharp's peak makes it to improve sensitivity and selectivity.

Fig. 6 displays the electrochemical responses of different concentrations of thermodynamically stable G-T and A-C mismatch targets. The resulting calibration curves are linear (inset) in the range of 10-1700 pM and 20 to 1200 pM with the detection limits 2 and 10 pM (3σ) for G-T and A-C mismatch targets, respectively. The signals are highly repeatable with a relative standard deviation of less than 5%. Therefore, the amplification of signals by using GR-AuNPs/GCE as a platform enables high sensitive simultaneous electrochemical detection of any possible SNPs. The linearity of calibration curve was verified using lack of fit test (Table S1). At the concentrations over ranges of 10-1700 pM for G-T and 20-1200 for A-C, the regression and linearity are acceptable. The values of Fisher ratio (1510.475 and 689.642 for G-T and A-C respectively) for regression were higher than the critical F-value (4.381 and 4.492) at α =0.05 and approved that the responses are significantly correlated to the concentrations. On the other hand, the values of Fisher ratio (1.488 and 1.869 for G-T and A-C respectively) for lacks of fit are lower than the critical F-value (2.958 and 3.259) at α = 0.05 and thus the linearity are acceptable as well.

4. Conclusion

A signal amplification strategy for improvement of our previously reported protocol for electrochemical SNPs genotyping using M-NPs [16] by applying GR-AuNPs /GCE platform is investigated in this manuscript and exhibits excellent sensitivity and selectivity for G-T and A-C mismatch targets, with detection limits as low as 2 and 10 pM, respectively. GR-AuNPs not only offer high surface area and good biocompatibility as an immobilization platform, but also GR with high electrical conductivity could enhance the electron transfer between DNA and the electrode. Table 1 shows a comparison between the present protocol and some other previously reported biosensors for genotyping of SNPs. This comparison demonstrates the present study for quantification of all SNPs is promising.

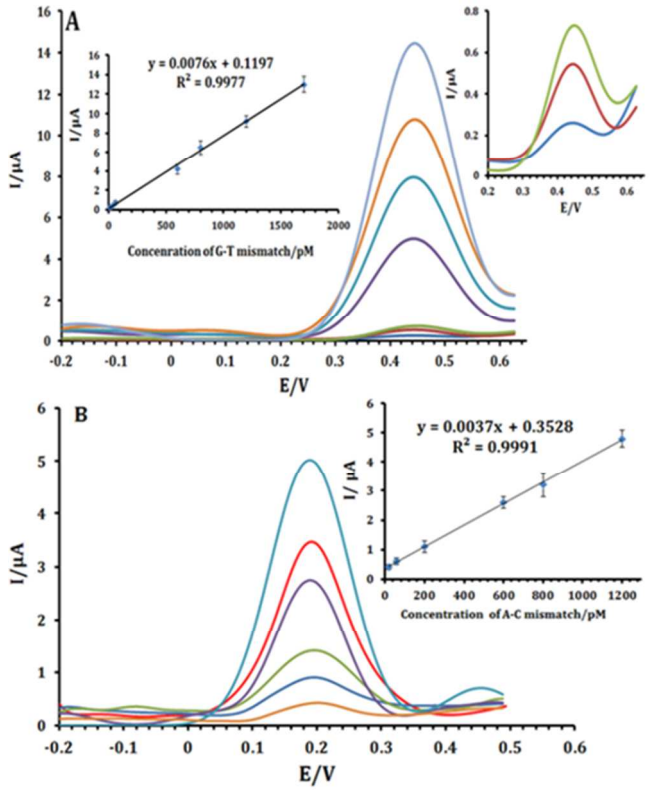

Fig. 6. DPV of oxidation DABA and AgNPs in different concentration of G-T (A) and A-C mismatch targets (B) on the GR-AuNPs/GCE and their calibration curves (insets).

Acknowledgement

We gratefully acknowledge the support of this work by the Esfahan University Research Council.

Notes and references

[a]Department of chemistry, University of Isfahan, Isfahan 81746-73441, Iran. +98 3117932710; fax: +98 3116689732. m.mehrgardi@chem.ui.ac.ir, m.mehrgardi@gmail.com (M.A. Mehrgardi)

1. J. Zhang, X. Wu, P. Chen, N. Lin, J. Chen, G. Chen and F. Fu, *Chem. Commun.*, 2010, **46**, 6986-6988.
2. S. Kim and A. Misra, *Annu. Rev. Biomed. Eng.*, 2007, **9**, 289-320.
3. P.-Y. Kwok and X. Chen, *Curr. Issues Mol. Biol.*, 2003, **5**, 43-60.
4. J. N. Wilson and E. T. Kool, *Org. Biomol. Chem.*, 2006, **4**, 4265-4274.
5. E. R. Mardis, *TIG*, 2008, **24**, 133-141.
6. S. C. Schuster, *Nat. Methods*, 2008, **5**, 16-18.
7. M. O. Dorschner, in *Genomic Applications in Pathology*, Springer, 2015, pp. 209-223.
8. T. Liu and J. K. Barton, *J. Am. Chem. Soc.*, 2005, **127**, 10160-10161.
9. A. A. Gorodetsky, A. Ebrahim and J. K. Barton, *J. Am. Chem. Soc.*, 2008, **130**, 2924-2925.
10. L. E. Ahangar and M. A. Mehrgardi, *Electrochim. Acta*, 2011, **56**, 2725-2729.
11. F. Patolsky, A. Lichtenstein and I. Willner, *Nat. Biotechnol.*, 2001, **19**, 253-257.

RSC Advances Accepted Manuscript

This journal is © The Royal Society of Chemistry 2012

12. G. Liu and Y. Lin, *J. Am. Chem. Soc.*, 2007, **129**, 10394-10401.
13. A. Abbaspour and A. Noori, *Biosens. Bioelectron.*, 2012, **37**, 11-18.
14. I. Willner, F. Patolsky, Y. Weizmann and B. Willner, *Talanta*, 2002, **56**, 847-856.
15. K. Kerman, M. Saito, Y. Morita, Y. Takamura, M. Ozsoz and E. Tamiya, *Anal. Chem.*, 2004, **76**, 1877-1884.
16. S. M. Khoshfetrat and M. A. Mehrgardi, *ChemElectroChem*, 2014, **1**, 779-786.
17. M. Ye, Y. Zhang, H. Li, Y. Zhang, P. Tan, H. Tang and S. Yao, *Biosens. Bioelectron.*, 2009, **24**, 2339-2345.
18. G. Liu, T. M. H. Lee and J. Wang, *J. Am. Chem. Soc.*, 2005, **127**, 38-39.
19. D. Lin, J. Wu, M. Wang, F. Yan and H. Ju, *Anal. Chem.*, 2012, **84**, 3662-3668.
20. F. P. Zamborini, L. Bao and R. Dasari, *Anal. Chem.*, 2011, **84**, 541-576.
21. M. A. Mehrgardi and L. E. Ahangar, *Biosens. Bioelectron.*, 2011, **26**, 4308-4313.
22. A. K. Geim and K. S. Novoselov, *Nat. Mater.*, 2007, **6**, 183-191.
23. W. Hong, H. Bai, Y. Xu, Z. Yao, Z. Gu and G. Shi, *J. Phys. Chem. C*, 2010, **114**, 1822-1826.
24. Y. Fang, S. Guo, C. Zhu, Y. Zhai and E. Wang, *Langmuir*, 2010, **26**, 11277-11282.
25. F. Li, H. Yang, C. Shan, Q. Zhang, D. Han, A. Ivaska and L. Niu, *J. Mater. Chem.*, 2009, **19**, 4022-4025.
26. S. WooáHan, *Chem. Commun.*, 2010, **46**, 3185-3187.
27. A. Shi, J. Wang, X. Han, X. Fang and Y. Zhang, *Sens. Actuators, B*, 2014, **200**, 206-212.
28. X. Han, X. Fang, A. Shi, J. Wang and Y. Zhang, *Anal. Biochem.*, 2013, **443**, 117-123.
29. Y. Hu, J. Jin, P. Wu, H. Zhang and C. Cai, *Electrochim. Acta*, 2010, **56**, 491-500.
30. L. Ruiyi, Z. Juanjuan, W. Zhouping, L. Zaijun, L. Junkang, G. Zhiguo and W. Guangli, *Sens. Actuators, B*, 2015, **208**, 421-428.
31. S.-J. Li, D.-H. Deng, Q. Shi and S.-R. Liu, *Mikrochim. Acta*, 2012, **177**, 325-331.
32. Y. Zheng, A. Wang, H. Lin, L. Fu and W. Cai, *RSC Advances*, 2015, **5**, 15425-15430.
33. S. Pruneanu, F. Pogacean, A. R. Biris, S. Ardelean, V. Canpean, G. Blanita, E. Dervishi and A. S. Biris, *J. Phys. Chem. C*, 2011, **115**, 23387-23394.
34. B. J. Sanghavi, P. K. Kalambate, S. P. Karna and A. K. Srivastava, *Talanta*, 2014, **120**, 1-9.
35. Q. Xue, Z. Liu, Y. Guo and S. Guo, *Biosens. Bioelectron.*, 2015.
36. D. Pan, Y. Gu, H. Lan, Y. Sun and H. Gao, *Anal. Chim. Acta*, 2015, **853**, 297-302.
37. W. Bai, H. Huang, Y. Li, H. Zhang, B. Liang, R. Guo, L. Du and Z. Zhang, *Electrochim. Acta*, 2014, **117**, 322-328.
38. J. Jiang, W. Fan and X. Du, *Biosens. Bioelectron.*, 2014, **51**, 343-348.
39. J. C. Claussen, A. D. Franklin, A. ul Haque, D. M. Porterfield and T. S. Fisher, *ACS Nano*, 2009, **3**, 37-44.
40. H.-L. Guo, X.-F. Wang, Q.-Y. Qian, F.-B. Wang and X.-H. Xia, *ACS nano*, 2009, **3**, 2653-2659.
41. Y.-G. Zhou, J.-J. Chen, F.-b. Wang, Z.-H. Sheng and X.-H. Xia, *Chem. Commun.*, 2010, **46**, 5951-5953.
42. M. S. El-Deab, *Electrochim. Acta*, 2009, **54**, 3720-3725.
43. S. M. Khoshfetrat and M. A. Mehrgardi, *Analyst*, 2014.
44. K. Shang, X. Wang, B. Sun, Z. Cheng and S. Ai, *Biosens. Bioelectron.*, 2013, **45**, 40-45.
45. Y. Xu, H. Bai, G. Lu, C. Li and G. Shi, *J. Am. Chem. Soc.*, 2008, **130**, 5856-5857.
46. Y. Wang, S. Zhang, D. Du, Y. Shao, Z. Li, J. Wang, M. H. Engelhard, J. Li and Y. Lin, *J. Mater. Chem.*, 2011, **21**, 5319-5325.
47. H. Wang, T. Maiyalagan and X. Wang, *Acs Catalysis*, 2012, **2**, 781-794.
48. X. Xie, J. Long, J. Xu, L. Chen, Y. Wang, Z. Zhang and X. Wang, *RSC Advances*, 2012, **2**, 12438-12446.
49. J. Luo, N. Zhang, R. Liu and X. Liu, *RSC Advances*, 2014, **4**, 64816-64824.
50. C. Xu, X. Wang and J. Zhu, *J. Phys. Chem. C*, 2008, **112**, 19841-19845.
51. L. Jiang, J. Qian, X. Yang, Y. Yan, Q. Liu, K. Wang and K. Wang, *Anal. Chim. Acta*, 2014, **806**, 128-135.
52. M. A. Raj and S. A. John, *RSC Advances*, 2015, **5**, 4964-4971.
53. A. B. Steel, T. M. Herne and M. J. Tarlov, *Anal. Chem.*, 1998, **70**, 4670-4677.
54. Y. Xu, M. Cao, H. Liu, X. Zong, N. Kong, J. Zhang and J. Liu, *Talanta*, 2015.
55. Y.-B. Tang, C.-S. Lee, J. Xu, Z.-T. Liu, Z.-H. Chen, Z. He, Y.-L. Cao, G. Yuan, H. Song and L. Chen, *Acs Nano*, 2010, **4**, 3482-3488.
56. J. Zhao, J. Wu, M. Zheng, J. Huo and Y. Tu, *Electrochim. Acta*, 2015.
57. M. Yang, J. Yao and Y. Duan, *Analyst*, 2013, **138**, 72-86.
58. Y. Li, Y. Yan, Y. Lei, D. Zhao, T. Yuan, D. Zhang, W. Cheng and S. Ding, *Colloids and Surfaces B: Biointerfaces*, 2014, **120**, 15-20.
59. Q. Xu, K. Chang, W. Lu, W. Chen, Y. Ding, S. Jia, K. Zhang, F. Li, J. Shi and L. Cao, *Biosens. Bioelectron.*, 2012, **33**, 274-278.
60. F. Gao, J. Lei and H. Ju, *Anal. Chem.*, 2013, **85**, 11788-11793.
61. X. Su, R. Robelek, Y. Wu, G. Wang and W. Knoll, *Anal. Chem.*, 2004, **76**, 489-494.
62. M. Cho, S. Chung, S.-D. Heo, J. Ku and C. Ban, *Biosens. Bioelectron.*, 2007, **22**, 1376-1381.
63. X. Mao, J. Jiang, X. Xu, X. Chu, Y. Luo, G. Shen and R. Yu, *Biosens. Bioelectron.*, 2008, **23**, 1555-1561.
64. D.-S. Xiang, K. Zhai and L.-Z. Wang, *Analyst*, 2013, **138**, 5318-5324.
65. H. Xu, L. Wang, H. Ye, L. Yu, X. Zhu, Z. Lin, G. Wu, X. Li, X. Liu and G. Chen, *Chem. Commun.*, 2012, **48**, 6390-6392.
66. T. G. Drummond, M. G. Hill and J. K. Barton, *Nat. Biotechnol.*, 2003, **21**, 1192-1199.
67. E. M. Boon, D. M. Ceres, T. G. Drummond, M. G. Hill and J. K. Barton, *Nat. Biotechnol.*, 2000, **18**, 1096-1100.

RSC Advances Accepted Manuscript